Heat flux and temperature evaluation in a rectangular multi-element GOX/GCH$_4$ combustion chamber using an inverse heat conduction method

Nikolaos Perakis[*†], *Maria Palma Celano*[*] *and Oskar J. Haidn*[*]
[*]*Institute of Turbomachinery and Flight Propulsion (LTF), Technische Universität München (TUM)*
Boltzmannstraße 15, 85748 Garching b. München, Germany
[†]Corresponding author

Abstract

The purpose of this study is to present an inverse heat transfer method which was developed and applied for the calculation of the heat flux and temperature profiles in an experimental multi-element rocket engine operated with GOX/GCH$_4$. The algorithm is based on an iterative optimization using a conjugate gradient method and utilizes the thermocouple measurements embedded in the material of the capacitively cooled combustor to provide an estimate for the hot gas heat flux. The method had been applied for the calculation of single-element engines by the authors[3] and has now been extended to include the more complex geometry of a combustor consisting of five injectors. The analysis presented in this work is based on experimental data obtained with the heat-sink rectangular engine at a pressure of 20 bar and various mixture ratios ranging from 2.6 to 3.4. The resulting temperature fields of the inverse method demonstrate a good agreement with the measurements and the injector footprint as well as transient effects during start-up are successfully captured. The key features of the heat flux results are further discussed in the paper.

Nomenclature

A	:	cross sectional area [m^2]	p	:	pressure [bar]
c^*	:	characteristic velocity [m/s]	$\mathbf{P}$	:	heat flux parameters [W/m^2]
c_p	:	specific heat capacity [J/(kg $\cdot$ K)]	PDE	:	partial differential equation
$CARS$	:	Coherent anti-Stokes Raman	$\dot{q}$	:	heat flux [W/m^2]
CEA	:	Chemical equilibrium with applications	R	:	recess length [m]
CFD	:	Computational Fluid Dynamics	T	:	temperature [K]
$\mathbf{d}$	:	direction of descent [W/m^2]	TUM	:	Technical University of Munich
D	:	diameter [m]	t	:	time [s]
FD	:	Finite Difference	$\mathbf{S}$	:	Jacobi matrix [K $\cdot$ m^2/W]
GOX	:	gaseous oxygen	x	:	horizontal coordinate [m]
GCH_4	:	gaseous methane	y	:	vertical coordinate [m]
I_{sp}	:	specific impulse	w	:	post wall thickness [m]
$ICHM$	:	inverse heat conduction method	z	:	coord. along chamber axis [m]
J	:	residual function [K^2]	α	:	convection coefficient [W/(m^2 $\cdot$ K)]
k	:	iteration number [-]	β	:	search step size [-]
$\dot{m}$	:	mass flow rate [kg/s]	γ	:	conjugation coefficient [-]
M	:	number of thermocouples [-]	ϵ	:	stopping criterion [K^2]
N	:	number of parameter points [-]	λ	:	heat conduction [W/(m $\cdot$ K)]
$NASA$	:	National Aeronautics and Space Administration	ρ	:	density [kg/m^3]
O/F	:	oxidizer to fuel ratio [-]			

1. Introduction

Over the past decades, significant effort has been placed in the numerical calculation of the combustion process in rocket engines. The necessity for a reliable prediction of the combustion characteristics and the heat loads within a combustion chamber and nozzle has promoted computational fluid dynamics (CFD) to become an integral part of the design process in the space propulsion industry. The validation of these numerical tools is usually done by comparing the calculated results for performance (I_{sp}, c^*), pressure profiles along the axial position ($p(z)$) as well as the heat flux values at the hot gas wall ($\dot{q}$). Of course this implies that trustworthy measurements with sufficient axial resolution for those values have to be available by the experiments over a wide range of operational conditions. The need for this data is even more critical for the innovative propellant combination of methane (CH$_4$) and oxygen (O$_2$) due to the limited number of available tests.[6,11]

Of the previously mentioned quantities, the one having the largest significance for the understanding of the physical and chemical phenomena is the heat flux. Due to the harsh environment within the chamber hot gas, the installation of sensors measuring temperature is almost impossible. Therefore, access to the burning gas is very limited and direct measurement is quite challenging and usually restricted to optical measurements of radicals' emission or to spectroscopic methods like the Coherent anti-Stokes Raman (CARS) spectroscopy. These methods however require the active film cooling of the optical window which can lead to an influence of the flow field. Due to these difficulties, a lot of information and especially insights regarding the characteristics of an injection system (its combustion properties, element/wall interaction) is done by taking a closer look to the heat flux distribution over the thrust chamber domain. The heat flux is hence used as a tool from which further information is deduced as far as the processes in the chamber are concerned. Moreover the prediction of the engine's lifetime, the design of an effective cooling system and the reliability of the chamber components after a specific number of tests is imminently connected to the heat loads applied onto the chamber wall thereby increasing the importance of this value even more.

The calculation of the heat flux in experiments where no active cooling system is present becomes challenging since the only information available consists of temperature readings at specific locations in the chamber material. To reconstruct the heat flux profiles requires the solution of an inverse problem. Methods used for single-element combustion chambers have already been developed and validated by Celano et al.[3] and Perakis et al.[14] but the literature focused on inverse methods of multi-element subscale chambers is limited. The present work provides a methodology for the calculation of heat flux distributions in multi-element combustors by utilizing an inverse method based on conjugate gradient optimization.

The code is applied on a 5-element subscale combustor which is operated at the Institute of Space Propulsion at the Technical University of Munich and runs with GCH$_4$ and GOX.

2. Experimental setup

In this section a description of the subscale rocket engine hardware and setup is presented. The multi-element combustor has a rectangular cross section with dimensions 48mm x 12mm, a chamber length of 277 mm and the contraction ratio is chosen at 2.5 to provide a Mach number of approximately 0.24, typical for rocket engine applications. The nozzle is a truncated trapezoidal prism with a rectangular throat section of 4.8mm x 48mm. The hardware along with the corresponding instrumentation is shown in Figure 1 and a detailed overview of its setup is also given in Celano et al.[2]

The injection system consists of five (5) identical coaxial injector elements placed next to each other along a line. This configuration is seen in the right sub-figure of Figure 1, where a cut-plane through the chamber is illustrated. Within this work, the thermocouples are numbered 1 to 5 starting from the left and going to the right. The distance between the injectors (center to center) is 6 mm and the injector-wall distance is 3 mm. For the test cases presented in this work, the GOX post is configured flush mounted with respect to the injection face. To ensure homogeneous injection conditions, in terms of temperature and pressure, two porous plates are placed in the oxidizer and fuel manifolds respectively. To characterize the injection conditions, thermocouples of type K and pressure transducers are installed in the chamber manifolds, prior to the porous plate. The main geometrical attributes of the injector elements are summarized in Table 1.

Because of the capacitive cooling of the combustor, the material used for the chamber and the nozzle segments is oxygen-free copper (Cu-HCP) chosen due to its high thermal conductivity. A large number of type T thermocouples with 0.5 mm diameter are installed in the chamber material at distances of 1 mm, 2 mm and 3 mm from the hot gas wall and kept in position by a spring loaded system. The axial resolution of the temperature sensors is 17 mm and in each axial plane a total of 7 sensors can be maximally installed. The locations of the 7 thermocouples are visible in Figure 1. The thermocouples are either located directly above an injector element (named with an index C) or in the middle between two elements (named with an index L or R depending on whether they are left or right of the reference
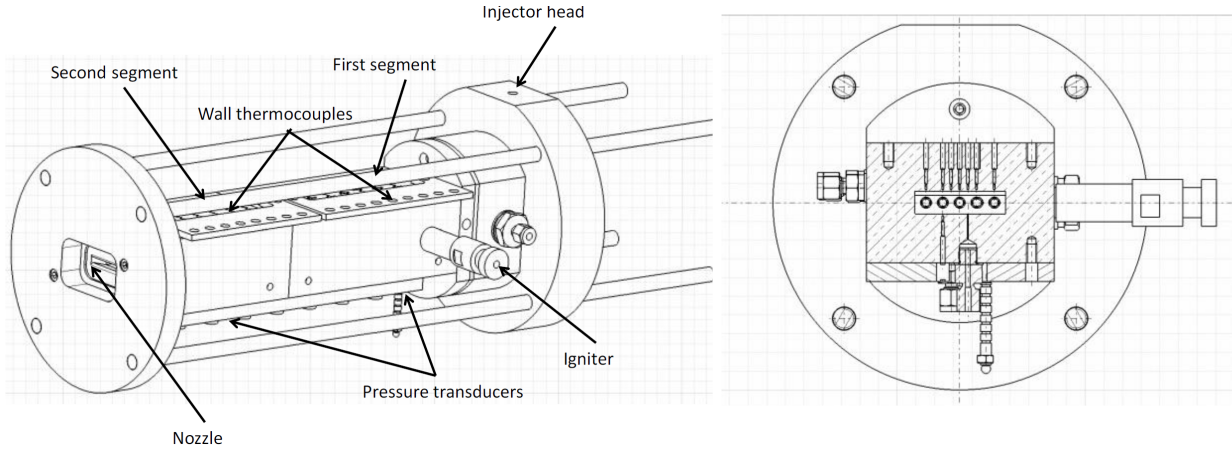
Figure 1: Multi-element combustion chamber.

Table 1: Injector dimensions.

GOX diameter D_{GOX}	4mm
GOX post wall thickness w	0.5mm
GOX post recess R	0mm
GCH$_4$ diameter D_{GCH4}	6mm
Injector area ration A_{GOX}/A_{GCH4}	0.7

element). Hence the names of the 7 thermocouples are 1C, 2C, 3L, 3C, 3R, 4C, 5C. Their positions along the x direction are summarized in Table 2 with x=0 corresponding to the center of the hot gas side. Not all potential thermocouples positions are occupied in every axial position: the number of sensors ranges with some planes containing a full set of 7, whereas others possess only 3 (e.g. 3L, 3C, 3R).

Table 2: Thermocouple positions.

Thermocouple name	x Position [mm]
1C	-18.0
2C	-9.0
3L	-4.5
3C	0.0
3R	4.5
4C	9.0
5C	18.0

Apart from the thermocouples, the pressure transducers provide additional information used to understand the combustion process of each test. Again an axial resolution of 17 mm is used and the WIKA A10 pressure sensors collect data at a rate of 100 Hz. The time evolution of the pressure profile in the O/F = 3.4 case is illustrated in Figure 2a by using the measurements of three sensors: one directly next to the faceplate, one at the middle of the chamber and one before the nozzle segment. The z coordinate has its origin at the face-plate and grows downstream of the injector. The pressure profiles for all three test cases are also shown in Figure 2b clearly demonstrating the static pressure loss due to the combustion process and the acceleration of the gases. The tests examined here are operated at a 20 bar [1] chamber pressure with different mixture ratios (O/F) of 2.6, 3.0 and 3.4. The different O/F values apart from altering the combustion characteristics, influence the mixing mechanism in the near injector region by modifying the velocity ratio and momentum flux ratio of the oxidizer and fuel streams.

---

[1] The nominal pressure of the test is 20 bar. Using the tool Chemical Equilibrium with Applications (CEA)[10] of NASA, the mass flow rates required to produce a pressure of 20 bar within the combustion chamber are calculated. During the test operation, these mass flow rates of oxidizer and fuel are applied but the resulting pressure does not always match exactly the nominal value, due to deviations of the real test from the idealized CEA calculation.
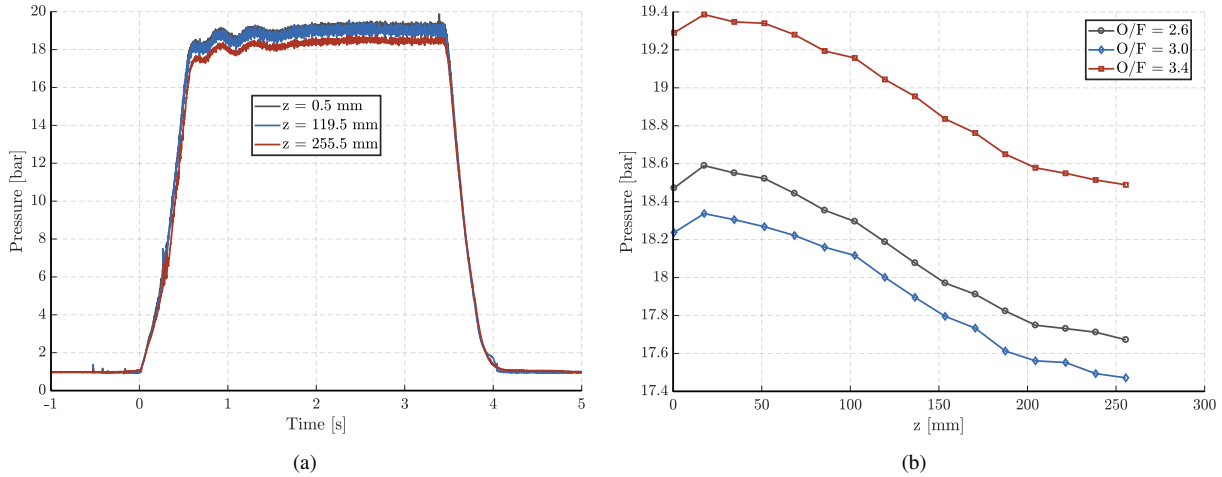
Figure 2: Time evolution of the combustion chamber pressure for the O/F = 3.4 case (a) and axial pressure profile for the three test cases (b).

Finally ignition in the combustor is achieved by a torch igniter using GOX and GCH$_4$ located on the side wall at a location around 34 mm downstream of the face-plate. The igniter runs at minimum power for 200 ms to limit its influence on the temperature readings.

With the information obtained via the temperature and pressure measurements, the goal is to determine the combustion properties and injector/injector interactions. To successfully achieve that, knowledge of the heat flux distribution on the inside wall is required. This is accomplished by means of an inverse heat conduction method (IHCM) which uses the thermocouple readings to deduce the heat flux in the chamber. The experimental data have also been presented and evaluated in Celano et al.[2] This paper hence focuses on the formulation of the inverse method and the additional information it can provide during the test evaluation process and less on the interpretation of the experimental values.

3. Inverse heat conduction method

Rocket engines cooled by a water cycle or other cooling medium have the characteristic property of reaching a steady state temperature distribution after the first seconds of operation. This effect is advantageous when evaluating the heat flux profiles, since they can simply be obtained from the enthalpy difference of the outgoing and incoming coolant flow. When dealing with capacitively cooled engines however, the temperature field is not stationary during the test operation and hence a transient inverse heat conduction method is needed. Several efforts have been performed to calculate the heat flux profiles in rocket engines,[5],[16] The main concept behind an inverse method for heat conduction problems lies in trying to estimate the boundary conditions (causes) which best fit the measured temperature values (effects) while keeping the physics of the problem intact.

Similarly to most inverse optimization algorithms, the method shown in the present work is based on an iterative approach as outlined in Figure 3. The goal of the optimization is to minimize the difference between the measured and calculated temperatures at the measurement locations. The program starts by initializing the temperature in the computational domain and choosing an initial guess for the heat flux. With the initial conditions (temperature field) and the boundary conditions (guessed heat flux) the first step is solving the direct heat conduction problem.

3.1 Direct solver

Although several commercial solvers exist able to handle this thermal conduction problem, a 3D finite difference (FD) code was developed specifically for this purpose by the authors and was validated in Celano et al.[3] and Perakis et al.[14] The implementation of the direct solver was carried out in Matlab to avoid any extra interfaces between the optimization code and the direct solver. A central difference approximation of the second derivative in the heat conduction equation (Eq. 1) was combined with an implicit Euler scheme for the time integration.
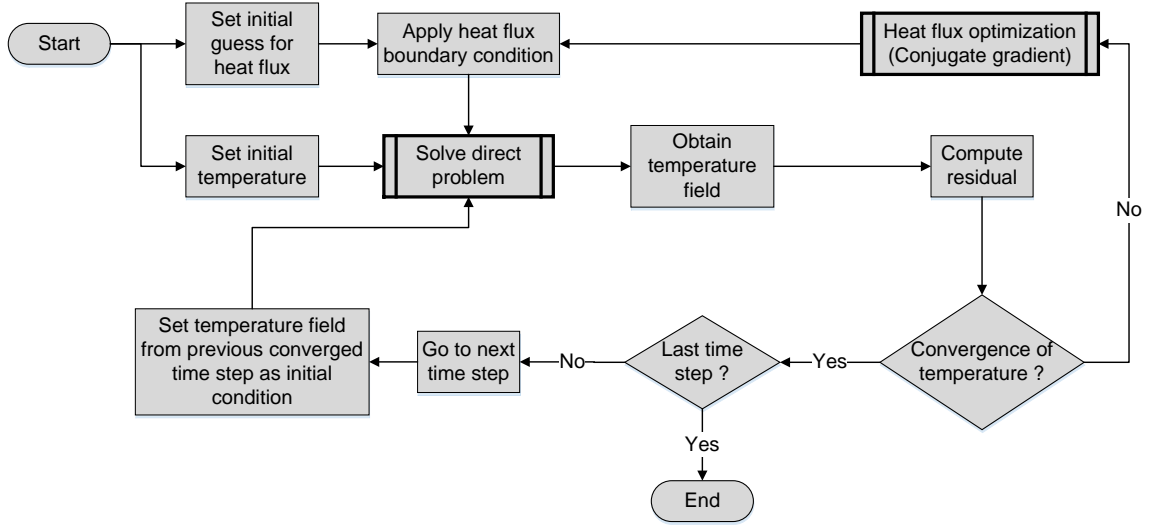
Figure 3: Inverse heat conduction iterative algorithm

$$\frac{\partial T}{\partial t} = \frac{\lambda}{\rho c_p} \nabla^2 T \tag{1}$$

The FD solver is used to solve the heat conduction partial differential equation (PDE) in a simplified geometry. The geometry consists only of the copper combustion chamber (excluding the nozzle segment) and is in principle a block with dimensions 64mm x 48mm x 272mm with a rectangular hole in the middle measuring 48mm x 12mm. For the material constants the typical values for oxygen-free copper are used (ρ = 8940 kg/m³, c_p = 393 J/(kg · K), λ = 385 W/(m · K)). Apart from the boundary condition in contact with the hot gas, which is the sought optimization variable, all the others are held constant over time and are modeled with von Neumann and Robin boundary conditions. Specifically, an adiabatic boundary condition is used for the face-plate and for the interface with the nozzle segment, whereas a natural convection boundary condition is applied to the outer wall with a convective heat transfer coefficient α = 10W/(m² · K) and an ambient temperature of 290 K.

Upon solving the direct problem, the temperature field after the end of the first time step is known. The calculated value of the temperature at all the thermocouple positions can hence be extracted and compared with the measured ones. This residual temperature difference is given as an input to the optimization algorithm.

3.2 Optimization method

The purpose of the optimization is to minimize the difference between the calculated ($\mathbf{T}_c$) and measured ($\mathbf{T}_m$) temperatures at each time step. This residual J which is subject to minimization is defined as in Eq. 2:

$$J(\mathbf{P}) = [\mathbf{T}_m - \mathbf{T}_c(\mathbf{P})]^T [\mathbf{T}_m - \mathbf{T}_c(\mathbf{P})] \tag{2}$$

The vector $\mathbf{P}$ describes the heat flux values at the parameter points which are subject to optimization. The heat flux is a continuous variable being applied to all the points, however optimizing the heat flux value at every single point in contact with the hot gas would be computationally expensive and subject to a larger error. The reason why errors could prevail easier is that having a larger number of optimization points increases the degrees of freedom of the problem without increasing the information input (no additional thermocouple measurements). Since inverse problems are ill-posed,[8] there are infinite solutions to them. Having a larger number of degrees of freedom would imply that there is also a larger number of physically irrelevant solutions which are not desired. For that reason, for the method presented here, a parameter is placed at every thermocouple position (projected on the hot gas wall), so the number of parameters N equals the number of thermocouples M. At each time step, the values of the N parameter points are

5

changed to reduce the residual J. Note that only thermocouples located at 1 mm distance from the hot gas wall are used.

Determining the amount by which each parameter value should be modified at every iteration is done by utilizing a conjugate gradient optimization method as described in Özisik.[13] This is done by means of the Jacobi matrix $\mathbf{S}$, which serves as a sensitivity matrix describing the change of the temperature at a thermocouple position due to a small change at a specific heat flux parameter value. Its structure is presented in Eq. 3.

$$\mathbf{S} = \begin{bmatrix} \frac{\partial T_1}{\partial P_1} & \cdots & \frac{\partial T_M}{\partial P_1} \\ \vdots & \ddots & \vdots \\ \frac{\partial T_1}{\partial P_N} & \cdots & \frac{\partial T_M}{\partial P_N} \end{bmatrix} \tag{3}$$

The compuation of the matrix occurs as a pre-processing step before the calculation and it is saved for future calculations as well. As long as the number and locations of the thermocouples and parameters does not change, the matrix remains unaltered.

After each iteration k, the values $\mathbf{P}^k$ are updated according to Eq. 4.

$$\mathbf{P}^{k+1} = \mathbf{P}^k - \beta^k \cdot \mathbf{d}^k \tag{4}$$

where β^k represents the search step size and $\mathbf{d}^k$ the direction of descent of the conjugate gradient method. Using the Fletcher-Reeves[9] expression for the conjugation coefficient and the gradient of the residual function from Eq. 5, the closure of the optimization algorithm is given by Eqs. 6 - 8 as described in Özisik.[13]

$$\nabla J(\mathbf{P}^k) = -2 \left[\mathbf{S}^k\right]^T \left[\mathbf{T}_m - \mathbf{T}_c(\mathbf{P}^k)\right] \tag{5}$$

$$\mathbf{d}^k = \nabla J(\mathbf{P}^k) + \gamma^k \mathbf{d}^{k-1} \tag{6}$$

$$\gamma^k = \frac{\sum_{j=1}^{N} \left[\nabla J(\mathbf{P}^k)\right]_j^2}{\sum_{j=1}^{N} \left[\nabla J(\mathbf{P}^{k-1})\right]_j^2} \tag{7}$$

$$\beta^k = -\frac{\left[\mathbf{S}^k\mathbf{d}^k\right]^T \left[\mathbf{T}_m - \mathbf{T}_c(\mathbf{P}^k)\right]}{\left[\mathbf{S}^k\mathbf{d}^k\right]^T \left[\mathbf{S}^k\mathbf{d}^k\right]} \tag{8}$$

The process is repeated until convergence is achieved, i.e. until the residual drops beneath a predefined value ϵ. When this is the case, the calculation of the next time step takes place while the temperature is initialized with the converged temperature field of the previous time step. The stopping criterion ϵ was chosen to be proportional to the precision of the thermocouple measurements ΔT, to the time step Δt and the number of the thermocouples M using an empirical constant C. Due to the inherent uncertainty of the thermocouple measurements, the error ΔT was set to 0.5 K, which is higher than the precision of type T thermocouples.

$$\epsilon = C \cdot M \left(\Delta T\right)^2 \Delta t \tag{9}$$

3.3 Applying the heat flux on the boundary

As mentioned in the description of the optimization algorithm, the heat flux is optimized only at specific locations and specifically only at the thermocouples' positions projected on the hot gas wall. Special care has to be taken to transform the heat flux from the few locations in the chamber to a continuous variable over the whole boundary domain. Each axial plane has the maximal capacity of accommodating 7 thermocouples at 1mm from the wall, at the locations 1C, 2C, 3L, 3C, 3R, 4C, 5C as described in Section 2, although most planes have a total of 3 thermocouples.

Along the x direction (horizontal side of the chamber), a special interpolating procedure has to be implemented. A simple linear interpolation between two neighboring parameter values is in most cases prone to error. This is because locations named with the index "C" are directly above an injector element and are expected to have higher heat flux values (at least for locations close to the face-plate where the flame temperature's stratification is more dominant) compared to the locations between the two injectors (for example 3L). Hence a linear interpolation between 4C and 5C would be overestimating the flux between the injectors.

For that reason the heat flux at positions where the thermocouples are missing, are taken by averaging the remaining values at the same plane. This means that the missing values between the injectors 4 and 5 are taken by averaging the heat flux at 3R and 3L. In an analog fashion if the thermocouples at a position above an injector element are missing (e.g. 5C), then the average of the remaining central thermocouples are taken (e.g. 3C and 2C). This interpolation method assumes that the heat flux profiles above each one of the 5 injectors are similar for a specific plane. If an axial plane has no thermocouples directly above an injector element or at a location between two elements, then the averaging cannot take place; instead an interpolation along the axial direction is done. If for example no central measurement is present (i.e. if all 1C, 2C, 3C, 4C and 5C sensors are missing), then the values for the position 4C are taken by interpolating with the values from the planes immediately upstream and downstram along the same x. After having defined the values at all locations directly above or between the injector elements, the values at all other nodes of the horizontal side are obtained by a cubic interpolation.

Only thermocouples at the upper wall are used and hence the heat flux profile at the down wall is defined identically to the upper wall, leading to a symmetric profile relative to the $y = 0$ plane. For the vertical walls of the hot gas side, a parabolic profile is defined. Since the distance between injector element and wall varies along the vertical wall (maximal at the corner and minimal at the middle of the side where $y = 0$), the heat flux is defined as a function of the vertical position as well. The corner value is known from the horizontal interpolation and the maximal value at the middle is defined as the average of the central values calculated for this plane (i.e. average of 1C, 2C, 3C, 4C, 5C). This can be used because the distance of the injector element from the vertical wall is the same as the one from the horizontal one, namely 3 mm.

4. Results

With those assumptions, the three test cases at a nominal operating pressure of 20 bar and O/F = 2.6, 3.0 and 3.4 were analyzed using the optimization code. Before comparing the three tests, the results of the 3.4 case will be shown in order to view the capabilities of the method.

4.1 Heat release

Firstly, the pressure and heat release profiles[2] are compared in Figure 4a. The two variables are connected to each other since the combustion process has the effect of both raising the pressure within the chamber as well as increasing the energy release and hence the integral heat load to the wall. The values for the heat release calculated by the code refer only to the combustion chamber, excluding the nozzle since no heat flux values are available. The pressure measurement used here corresponds to the sensor located close to the face-plate, i.e. at z=0.5 mm.

It is observed that the heat release starts increasing approximately at the same instant as the pressure at t=0 s. After a sharp rise for the first 250 ms, the heat release increase seems to slow down at t=0.25 s. The pressure profile also measures a small oscillation at the same time. The effect is attributed to the end of the igniter operation, which leads to a slight hold in the increase of the energy release. During the operation of the igniter, the presence of an additional transversal jet influences the injector flame, due to a local increase of mixing and therefore higher heat release, which is explained by the peak of the heat flux close to the face plate. This effect has been also observed for the single element chamber as described in Silvestri et al.[15] Immediately after the influence of the igniter is damped away, the energy release in the chamber continues to increase along with the pressure signal and reaches a constant plateau around the t=1.5 s mark. Looking at the pressure signal, one notices that the pressure demonstrates a small oscillation from t=0.6 s

---

[2]Here the term "heat release" refers to the heat loss through the wall and not to the total heat released within the chamber.

until t=1.5 s. The cause of this transient phenomenon could be that the anchoring of the flame in all five injector elements does not happen simultaneously. The elements close to the igniter source are the ones being stabilized faster and the flame propagates to the others slightly later. When the flame is attached and stable, then a constant pressure level is expected. This is also the case at t=1.5 s, which coincides with the time point at which the heat load gets to a plateau as well. Hence the inverse method is able to capture the qualitative transient development of the heat loss through the wall, which is verified by the pressure signal.

Apart from the time evolution of the integrated heat flux over the chamber area, examining the heat flux profile over time at specific locations in the chamber also gives information about the combustion characteristics. In Figure 4b, the temporal profile of the heat flux at the 3C location for two different axial planes (z=34.5 mm and z=272.5 mm) is plotted. The heat flux values have been normalized with their respective maximal value in order to emphasize the qualitative effect of the time evolution without taking into account the effect of the difference in absolute value. The values at z=34.5 mm demonstrate a peak after around 0.25 s before reaching a constant level. As explained earlier, this is the effect of the igniter which is located at the same axial position. The results further downstream right before the nozzle segment (z=272.5 mm) seem to be uninfluenced from the igniter effect, since there is no peak present along time. This behavior is expected since start-up effects should be located close to the ignition source and should have disappeared before reaching the end of the combustion chamber.
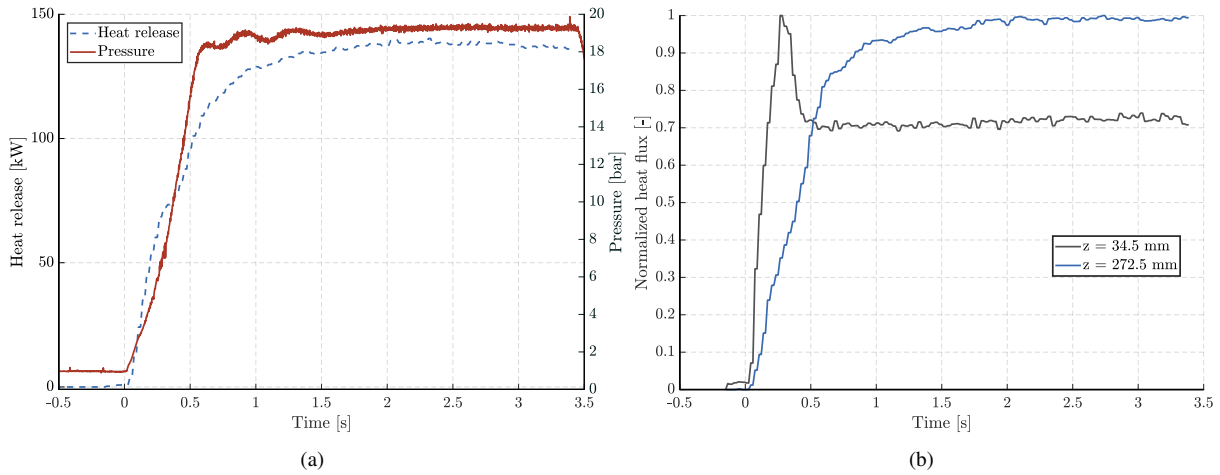

Figure 4: Time evolution of chamber pressure, heat release (a) and normalized heat flux (b).

4.2 Temperature and heat flux along horizontal position

The main difference between an inverse method used for the heat flux evaluation in a multi-element chamber compared to a single element one is the azimuthal variation of the heat flux profile. In the case of a rectangular combustor as in this case, the variation occurs along the x axis. In order to examine the capability of the method to predict the heat flux variation along the horizontal hot gas wall, the temperature profiles at 1 mm distance from the wall for some selected axial positions (Figure 5) and the corresponding heat flux values (Figure 6) are examined.

In Figure 5, the measured values are indicated with symbols and the solid line represents the calculated values stemming from the inverse method. The results are shown at the end of combustion operation (t=3.3 s). The planes at z=51.5 mm, z=102.5 mm and z=153.5 mm are equipped with all seven thermocouples, whereas at z=170.5 mm and z=255.5 mm only the 3L, 3C and 3L positions are filled. The outer left position corresponds to 1C and the far right one to 5C as summarized in Table 2. Starting with the plane closest to the face-plate (z=51.5 mm) one notices that the temperature values directly above the injector elements (2C, 3C and 4C) are higher than the measurements between the injectors (3L, 3R). This is also captured in the heat flux profile for the same plane, which demonstrates peaks at the positions 1C, 2C, 3C, 4C and 5C and lower values at the locations in between. This effect of temperature stratification and specifically of higher heat release directly above the elements is expected close to the face-plate where the individual streams have not been mixed and the flow-field can be imagined as five separate cylindrical flames.

The same pattern of maximal heat flux values at the "C" locations is observed at the planes z=170.5 mm and z=255.5 mm as shown in Figures 5 and 6. However, planes z=102.5 mm and z=153.5 mm show the exact opposite effect, with the heat flux values between the injectors being higher than directly above the elements. This results can be deduced by simply looking at the 3L, 3C and 3R temperature measurements for these planes. The effect of the shift
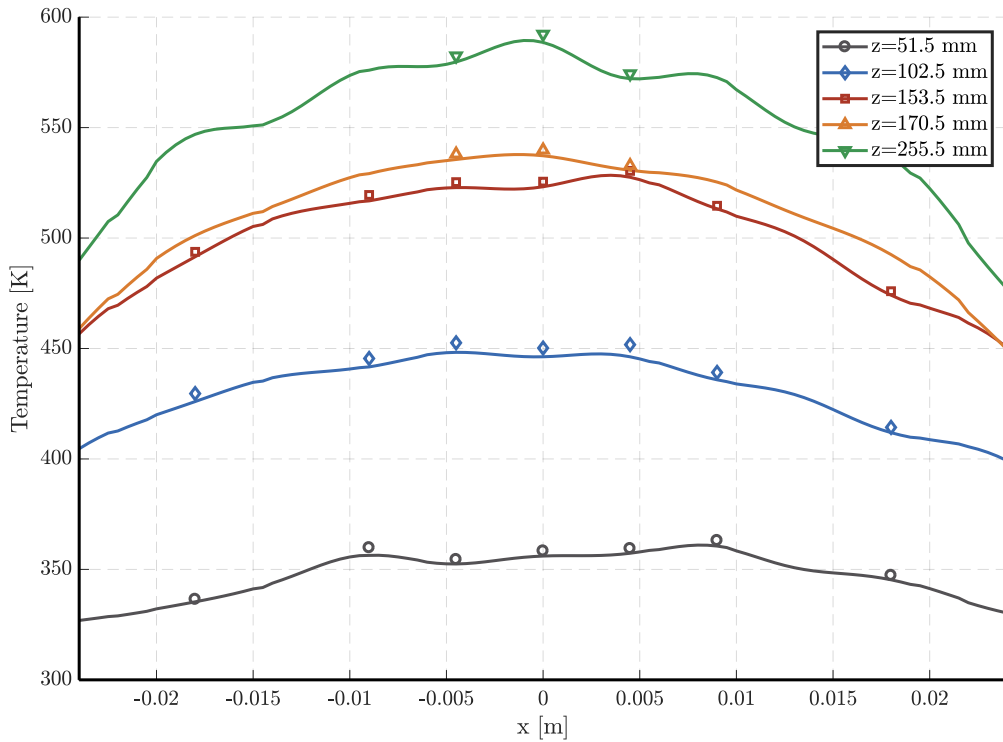
Figure 5: Temperature at 1 mm from the hot gas wall over x position at t = 3.3 s.
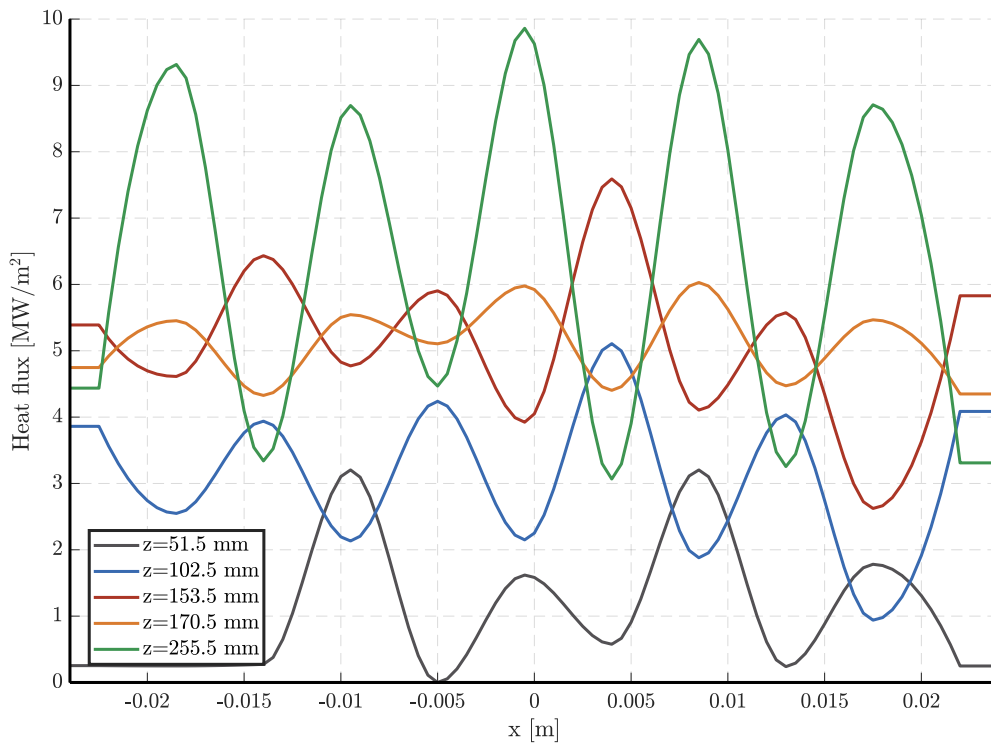

Figure 6: Heat flux over x position at t = 3.3 s.

in the maximal heat flux azimuthal position has been observed in other subscale engines as well. CFD simulations by Perakis[12] preformed on the ISP-1 subscale combustor[7] showed that downstream of a specific location at the chamber, the heat flux values above the injector elements were lower than the ones between two elements of the outer row. This effect was attributed to the presence of unburnt oxygen on the wall which had a lower conductivity than the

9

burnt products thereby reducing the heat flux. It is assumed that a similar process takes place in the case of the TUM rectangular combustor.

For positions further downstream than this "shifted" peak, it is expected that the heat flux should be smoother along the x direction, with fewer variations between the maximal and minimal values due to an increase in mixing, leading to a smaller stratification degree. This is indeed observed at the z=170.5 mm where the differences between the heat flux values remain underneath $1\,\mathrm{MW/m^2}$. This is also depicted in the temperature profile which almost has the form of a parabola, with very small variations. In general, observing the trend for all four planes up to the z=170.5 mm location, one sees that the stratification decreases indicating a better mixing of the hot gas.

However the plane at z=255.5 mm demonstrates a further increase in stratification and larger variations of the thermocouple readings and hence obtained heat flux values. Since this would correspond to a decrease in the mixing degree of the burnt gas compared to positions further upstream, the results have to be treated with caution. A possible explanation for this behavior could be a problem with the installation of the thermocouples. If the thermal contact between sensor and chamber material is not adequate then a bigger response time and hence slower measurement can be expected. This could be the case for the 3L and 3R sensors in this plane. Also the sensitivity of the thermocouples' distances from the hot gas wall is also an issue. If the position deviates from the nominal 1 mm, then due to a high sensitivity of the calculated heat flux on the measurement, a bigger heat flux error has to be accounted for. Nevertheless, some aerodynamic effects could also influence the heat release in this part due to the presence of the truncated nozzle. Due to the sharp edge and the presence of more chamber material at this location, a more detailed CFD analysis is required to fully understand the dynamics of heat release close to the end of combustion. Therefore CFD simulations are also planned to examine whether this effect could be physically possible or if it is a byproduct of the hardware installation.
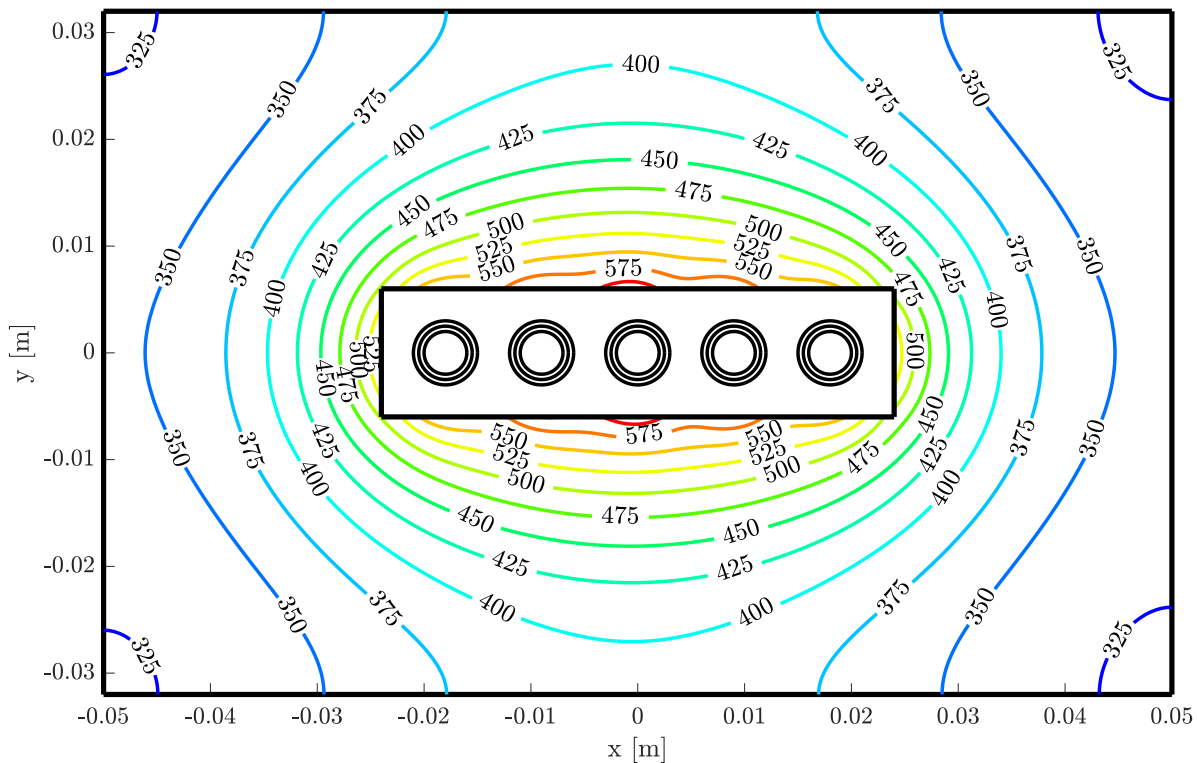

Figure 7: Temperature field at the plane 272.5 mm downstream of the injector at t = 3.3 s.

The high sensitivity of the thermocouple position on the obtained heat flux profile can be grasped by examining Figure 7. Here the temperature field at the last axial plane before the nozzle is plotted at t=3.3 s. The isolines close to the hot gas wall (within the first 2-3 mm) show a "wavy" pattern indicating the variation of the heat flux along the axial position. For distances farther away however, the temperature variation seems to vanish and the isolines show a nearly elliptical form. This implies that positioning the thermocouples in a smallest possible distance from the chamber wall is needed for accurate heat flux evaluation. This also implies that a small deviation of the thermocouple from the nominal position or a faulty thermal contact would produce a large heat flux uncertainty because of the high sensitivity.

4.3 Validation of heat flux level

So far the results of the inverse method were examined from a qualitative point of view and it was demonstrated that the transient profiles as well as the horizontal distribution of temperature and heat flux were able to capture some physical effects. However no comments were made regarding the absolute value of the heat flux.

The first estimation regarding the heat flux value expected in the combustion chamber can be made by comparing with a single element rocket combustor operated with gaseous methane and oxygen which was designed and tested at the TUM.[2,4] It is expected that since the same injector elements are used both for the single and the multi-element chamber and since the contraction ratios are also identical (to ensure same Mach numbers in the chamber), tests at the same pressure level and O/F should give similar heat flux levels. This can be directly deduced by taking a look at the Bartz formula,[1] which gives an estimate of the convective heat transfer coefficient α_g.

$$\alpha_g \propto \frac{1}{D^{0.2}} \left(\frac{D_t}{D}\right)^{1.8} \left(\frac{p_c}{c^*}\right)^{0.8} \tag{10}$$

For the derivation of this simplified formula, it has been assumed that the Prandtl number and gas properties (viscosity, specific heat capacity, adiabatic combustion temperature) for the two configurations are identical, which is close to reality. For the same operating point, the combustion pressure p_c and the characteristic velocity c^* are also constant and since the two chambers have equal contraction ratios, the term $\left(\frac{D_t}{D}\right)^{1.8}$ equals unity [3]. This implies that the average convective heat transfer coefficient (and therefore the heat flux if the same wall temperature is assumed) are given by:

$$\dot{q}_{multi} = \dot{q}_{single} \cdot \left(\frac{D_{single}}{D_{multi}}\right)^{0.2} \approx 1.10 \cdot \dot{q}_{single} \tag{11}$$

The expected profiles should be similar, with the multi-element chamber having a slightly higher value. This is verified when comparing the average heat flux profiles along the axial position as in Figure 8a. An interpretation of the profile's shape is given in Celano et al.[2] Here, the figure is merely used to prove that the maximal heat flux value (approximately $6.5\,\mathrm{MW/m^2}$) is close to the one of the single-element one and in fact approximately 10% higher, as the Bartz formula predicted. Since the code for the single-element chamber has been validated in Celano et al.,[3] a validation of the absolute heat flux value for the inverse method presented here was carried out.

A further step to validate the axial profile of the average heat flux was made by comparing with a calorimetric method for the same chamber. The multi-element chamber developed at the TUM can be operated either in capacitive or in water-cooled mode. This is enabled by the modular form of the chamber segments which can be interchanged. In the water-cooled configuration, the segments are equipped with cooling channels which can be flown either counterflow or in co-flow with the hot gas. This makes a measurement of the heat flux based on the enthalpy difference of in- and outflowing water possible. A test at O/F=3.4 and pressure of 20 bar was repeated with the cooled hardware and the heat flux results are shown in Figure 8b. Seven separate segments are present, which give the average heat flux for each one of them. In order to perform the comparison, the results from the inverse method were also averaged along the same positions. It can be observed that the two curves demonstrate the same trend and have a difference of less than 5% in the segments located close to the middle of the chamber.

Planes closer to the nozzle show a higher deviation. This is attributed to the boundary condition applied in the inverse method. The boundary before the nozzle is treated as an adiabatic wall. Of course, since the heat flux at the nozzle segment is the highest, it is expected that the material at this point has a higher temperature and hence that an axial heat flux contribution flowing upstream (backwards) would heat up the last planes before the nozzle. With the adiabatic boundary condition applied, the code attributes the temperature increase in the last planes solely to heat stemming from the chamber and hence slightly overestimates this value. In order to improve this effect, an axial heat flux value will be imposed in the future to represent the nozzle influence.

The calorimetric method also contains some uncertainty and a higher number of tests is required to quantify the experimental error. Moreover, although efforts are made that the two hardware configurations (capacitive and water-cooled) are identical, it is still two different chambers and some discrepancies in the results could be attributed to this fact. The general trend however of the two methods is in good agreement, serving as a first validation of the multi-injector inverse code.

---

[3]The characteristic velocity is dependent on the O/F and operating pressure, as well as the integral heat loss to the wall. For this simplified approach, we simply wish to show that the two chambers should have the same order of magnitude heat flux level and not to exactly calculate the heat flux of the multi-element combustor based on the analogy. Therefore the change in c^* is neglected here.
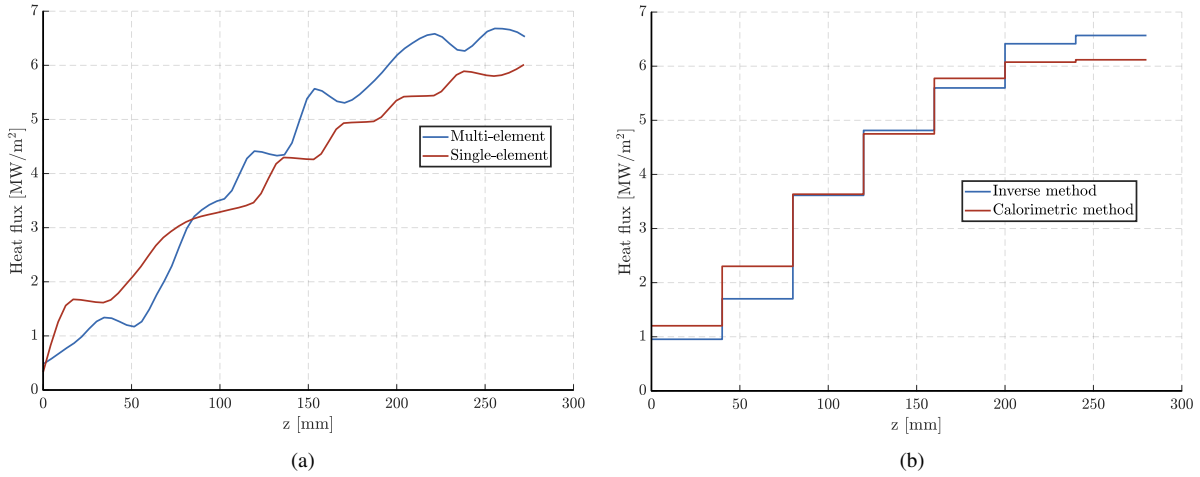
Figure 8: Comparison between multi-element and single element heat flux results (a) and between the inverse and calorimetric methods' heat flux profiles (b) for the O/F=3.4, 20 bar test case.

4.4 Comparison of different operating points

In order to have a qualitative comparison between different test cases, apart from the results for the O/F=3.4 case which have been shown so far, two tests with O/F=2.6 and O/F=3.0 were also evaluated. The time-dependent profiles of the heat release are shown in Figure 9. All three test cases appear to reach a steady state heat rate at around the same time point. The level of the heat release is higher for the 3.4 case and the lowest for the 2.6 test. This is attributed to two factors: the test with O/F=3.4 is closest to the stoichiometric point and hence a larger energy release and combustion temperature is expected. Moreover the pressure level for the 3.4 case was slightly higher as can be seen in Figure 2 which contributed to the higher heat flux values. The inverse method hence seems to be able to provide qualitatively physically relevant results for the heat flux profiles.
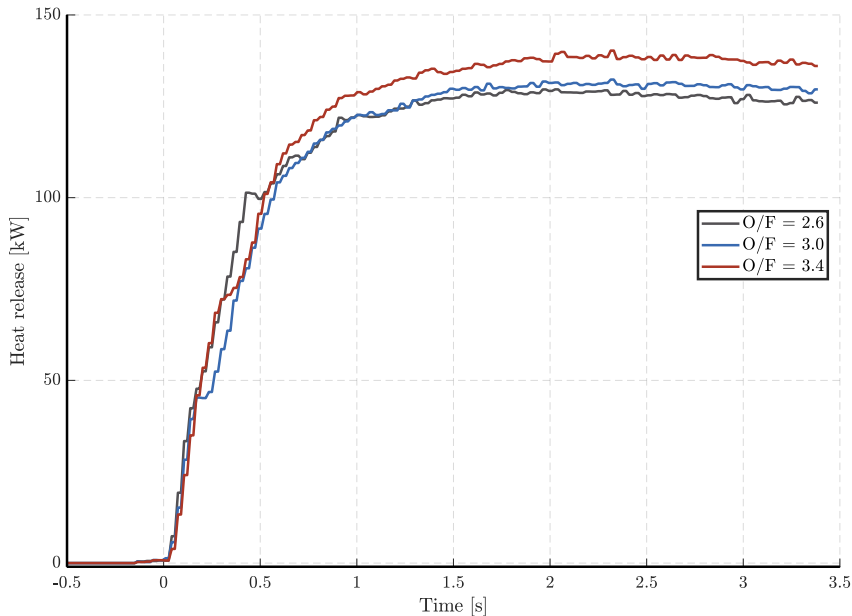

Figure 9: Integrated heat loss to the wall at t = 3.3 s.

Furthermore, the axial profiles of temperature at 1 mm and heat flux are compared in Figure 10. The values of the temperature correspond to the 3C injector position, whereas the heat flux is the average value for each axial position. The fact that the 3.4 test case has a higher heat flux can be already speculated by looking at the temperature values, which are higher for this load point. This is predicted in fact by the inverse method which delivers a higher heat flux

level for the positions downstream of the face-plate.

Interestingly the temperature and heat flux values for the first 60 mm after the injector plate are higher for the 2.6 case and the lowest for the 3.4 test. This is physically explained by the fact that the velocity of the methane for the 3.4 is the lowest among the 3 test points. This implies that the annular CH$_4$ jet is pulled inward by the faster O$_2$ jet due to shear forces, thereby increasing the distance of the flame front from the wall. In contrast, the 2.6 case has the highest fuel velocity which means that the inner oxidizer jet is pulled outward and the distance between flame and wall is reduced. Farther downstream where the initial mixing effect is damped out and the energy release increases, the heat flux and temperature values rise and become the highest for the 3.4 load point because it is closer to the stoichiometry (hence has a higher total energy release).

The general trend for the axial profile of the heat flux is captured since the inverse method predicts an increasing heat flux level along the z axis which reaches a plateau at around 220 mm from the face-plate. The point at which the almost constant value establishes itself marks the end of combustion. Since no further energy release takes place, it is expected that the heat loss to the wall also remains constant. This fact is also supported by the pressure transducers' readings as illustrated in Figure 2. At the z=210 mm axial position, the profiles of all three load points seem to flatten out, indicating that no further acceleration of the fluid is present, which also implies the end of combustion processes.

However some oscillations are observed along the z axis. In fact at positions where the temperature profile has an inflection point (50 mm, 100 mm, 170 mm) the heat flux appears to have a local minimum. This can also be observed at Figure 6, where some planes demonstrate lower heat flux values compared to planes upstream, which corresponds to a "bump" along the axial direction. Since no physical explanation for such an unsteady behavior could be found, the oscillation is attributed to numerical reasons and specifically the interpolation method between the axial planes. There are infinite solutions to an inverse problem and the one found by the code and presented here is one of them. Because the optimization occurs almost independently between each plane, it happens that some discontinuities appear (in the form of bumps or oscillations) along the axial direction.
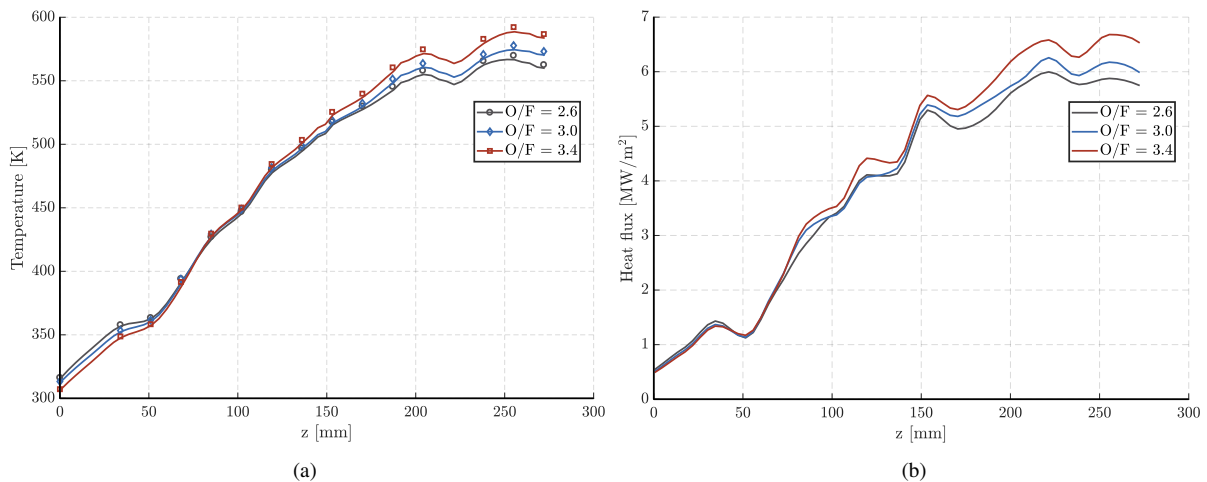

Figure 10: Profile of temperature at 1 mm distance from the hot gas wall in the 3C position (a) and average heat flux (b) along the axial position at t = 3.3 s.

The observed phenomenon could also be a result of different response times of the thermocouples or different thermal contact. The same profiles over axial position are also plotted at t=1.3 s in Figure 11 and one can observe that the temperature field does include some oscillations itself which are picked up by the inverse method. It is therefore not clear if the inverse method produces the oscillations because they are dictated by the temperature field itself or if they appear because of a non-optimal interpolation method. A further analysis of the hardware and an improvement of the interpolation scheme will be carried out to improve the profiles. Predictions of the heat flux level and the general profile trend are however still reliable as the results presented here have demonstrated.

5. Conclusion

An inverse heat flux evaluation method based on a conjugate gradient method has been applied successfully to reconstruct the heat flux and temperature profiles inside a rectangular multi-element rocket combustion chamber. The inverse method had previously been utilized to predict heat flux values in single element combustors operated with
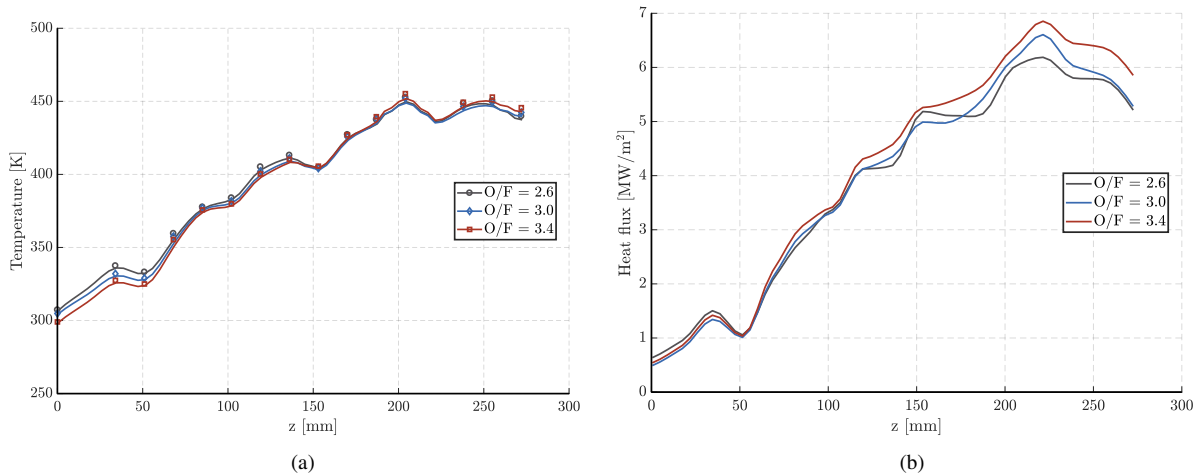
Figure 11: Profile of temperature at 1 mm distance from the hot gas wall in the 3C position (a) and average heat flux (b) along the axial position at t = 1.3 s.

GCH$_4$/GOX and was extended by the authors to include more complex geometries with multiple elements.

For the verification of the method, a GCH$_4$/GOX test case operated at 20 bar and O/F=3.4 was examined. Comparing the transient profiles of the pressure signal and the heat release in the combustion chamber, qualitatively similar trends were observed and especially the effect of the ignition system was evident in both profiles. Moreover the influence of the igniter transient was dominant in the heat flux results of the planes close to the torch whereas positions farther downstream showed a smoother effect over time. Using results from a water-cooled version of the same chamber served as a further validation of the average heat flux results along the axial direction.

An important benefit of the inverse method in the case of a multi-element chamber is being able to capture the injector footprint based on the thermocouple measurements. The temperature measurements and hence the resulting heat flux values showed that the stratification among the five injectors is reduced with increasing distance from the face-plate. Some planes however close to the nozzle show an increased stratification which cannot be physically explained and is attributed to a faulty installment of the thermocouples. A shift of the maximal heat flux value is also observed: for some planes the maximal heat flux value occurs directly above the thermocouple elements whereas in others the values in the middle between two elements are the highest. This behavior will be investigated further using CFD analysis of the chamber.

Finally, oscillations of the heat flux values along the axial direction were observed. It is still unclear whether the nature is pure numerical or if the potentially different response times of the thermocouples contribute to it. The high sensitivity of the heat flux values on the measured temperatures requires an efficient interpolation of the boundary values to ensure that a physical solution is met. Different interpolation schemes between the axial planes will be analyzed in order to make the method more robust and potentially produce a more physical, oscillation-free solution.

6. Acknowledgments

References

[1] D. R. Bartz. A simple equation for rapid estimation of rocket nozzle convective heat transfer coefficients, 1957.

[2] M. P. Celano, S. Silvestri, C. Bauer, N. Perakis, G. Schlieben, and O. J. Haidn. Comparison of single and multi-injector GOX/CH4 combustion chambers. In *52nd AIAA/SAE/ASEE Joint Propulsion Conference*, AIAA 2016-4990.

[3] M. P. Celano, S. Silvestri, J. Pauw, N. Perakis, F. Schily, D. Suslov, and O. J. Haidn. Heat flux evaluation methods for a single element heat-sink chamber. In *6th European Conference of Aeronautics and Space Science, Krakow, Poland*, 2015.

[4] M. P. Celano, S. Silvestri, G. Schlieben, C. Kirchberger, O. J. Haidn, and O. Knab. Injector characterization for a gaseous oxygen-methane single element combustion chamber. In *Progress in Propulsion Physics*, volume 8, pages 145–164. EDP Sciences, 2016.

[5] E. B. Coy. Measurement of transient heat flux and surface temperature using embedded temperature sensors. *Journal of Thermophysics and Heat Transfer*, 24(1):77–84, 2010.

[6] F. Cuoco, B. Yang, and M. Oschwald. Experimental investigation of LOX/H2 and LOX/CH4 sprays and flames. In *24th International Symposium on Space Technology and Science*, 2004.

[7] Suslov D. ISP-1: Deliverable 2.6.

[8] Artioukhine E. Heat transfer and inverse analysis. *RTO-EN-AVT-117*, 2005.

[9] R. Fletcher and C. M. Reeves. Function minimization by conjugate gradients. *The Computer Journal*, 7(2):149–154, 1964.

[10] S. Gordon and B. J. McBride. Computer program for calculation of complex chemical equilibrium compositions and applications. part 1: Analysis. 1994.

[11] J. Lux, D. Suslov, M. Bechle, M. Oschwald, and O. J. Haidn. Investigation of sub-and supercritical LOX/methane injection using optical diagnostics. *42nd AIAA/ASME/SAE/ASEE Joint Propulsion Conference & Exhibit*, AIAA 2006-5077.

[12] Perakis N. Flamelet modeling and simulation of CH4/O2 rocket thrust chambers. *Technical University of Munich*, Master's thesis, 2016.

[13] M. N. Özisik. *Inverse Heat Transfer: Fundamentals and Applications*. CRC Press, 2000.

[14] N. Perakis, L. Werling, H. Ciezki, and S. Schlechtriem. Numerical calculation of heat flux profiles in an N2O/C2H4 premixed green propellant combustor using an inverse heat conduction method. In *Space Propulsion Conference*, 2016.

[15] S. Silvestri, M. P. Celano, G. Schlieben, C. Kirchberger, and O. J. Haidn. Characterization of a GOX-GCH4 single element combustion chamber. In *4th Space Propulsion Conference, Köln (Germany)*, 2014.

[16] A. Vaidyanathan, J. Gustavsson, and C. Segal. One-and three-dimensional wall heat flux calculations in a O2/H2 system. *Journal of Propulsion and Power*, 26(1):186–189, 2010.